Environ. Sci. Technol. 1998, 32, 3293–3298

Measuring Partition Coefficients of Colloids at Air–Water Interfaces

JIAMIN WAN* AND TETSU K. TOKUNAGA
Earth Sciences Division, E. O. Lawrence Berkeley National Laboratory, Berkeley, California 94720

Quantification of surface excesses of colloidal particles at gas–liquid interfaces under environmentally relevant conditions has not previously been reported, despite its importance in understanding and predicting partitioning, transport, and transformations of colloids and other organic and metal species complexed onto colloids in many natural environments and engineered systems. In this study, we developed a bubble column method for measuring partition coefficients of colloids at air–water interfaces. The method was validated by comparing the adsorption isotherm constant for a surfactant measured using our method with that determined from conventional surface tension measurements and the Gibbs absorption equation. The first measured partition coefficients of kaolinite and humic colloids at the air–water interfaces are reported. The bubble column method can also be used to identify surface exclusion of colloids at the air–water interface. By extension, this method will permit quantification of surface activities of a wide range of inorganic, organic, and microbial colloids as well as molecular species complexed onto colloids.

Introduction

Colloidal particles include many different organic, inorganic, and microbial substances. Their very small sizes (nm to μm) give them high specific surface areas and often high surface charge densities. These characteristics make suspended particles efficient carriers of otherwise immobile, strongly sorbing metal ions. In addition to their well-known mobility in water, particles are also found to favorably accumulate at air–water interfaces in many natural environments and engineered systems. Ocean and lake surfaces play important roles in transport and transformations of many physical, chemical, and biological entities. Enrichment of particle-associated heavy metals and organic compounds has been found at the surface of oceans and lakes (*1–6*). For instance, the concentrations of lead, iron, nickel, copper, fatty acids, hydrocarbons, and chlorinated hydrocarbons were found to be 1.5–50 times higher in the surface layer (approximately 150 μm thick) of Narragansett Bay relative to the bulk water, with most of the enrichment in the particulate and organic fractions (*2*). Clays, humic acids, and microorganisms have been found accumulated at air–water interfaces in unsaturated soils (*7–10*). Engineered systems such as flotation-based mineral separation methods also take advantage of particle partitioning at air–water interfaces (*11*). These examples suggest that colloidal partitioning at air–water interfaces can be significant in a wide variety of natural and engineered systems. For surface active molecules, changes in surface tension with changes in solution concentration determine their surface excesses through the Gibbs equation (*11*). However, for suspensions of particles, surface tension changes are often not measurable. In this paper, colloid particle surface excesses are defined in a manner similar to that used for dissolved molecules. This quantity is the excess number of particles per unit interfacial area relative to that obtained by assuming that the bulk suspension concentration extends unchanged up to the air–water interface. In this study, we focus on a quantification method that can be used in future studies concerning mechanisms responsible for colloid partitioning at liquid–gas interfaces. Much effort has already been devoted to characterizing surface accumulations of particles and associated species. The methods developed include surface microlayer sampling (using stainless steel mesh, skimmer devices, or germanium slides) and jet drop collection (*3, 12–14*). Because of the uncertain thicknesses and interfacial areas sampled in these methods, results are often reported as the enrichment factors for a given estimated thickness. In this study, a simple dynamic method was developed to quantify particle surface excesses at air–water interfaces without requiring measurements or assumptions concerning the thickness of interfacial regions.

Theory

Determining the Partition Coefficient. We developed a method using a bubble column device for quantifying colloidal surface excesses. In the bubble column system, gas is bubbled through a vertical column containing the dilute aqueous suspension (or solution) of the colloids (or solute), with an open free surface at the top. The rising bubbles sorb and carry the surface-active species upward and then release them back to the solution at the free surface where the bubbles burst. At steady-state, a concentration profile is established along the column length that reflects the balance between upward transport by partitioning onto rising bubbles and downward transport by eddy dispersion. By predetermining the column eddy dispersion coefficient for given conditions (column dimensions, air flow rate, and bubble size) and measuring the steady-state concentration profile, the partitioning between bulk and surface regions can be determined. Lemlich (*15, 16*) and Shah and Lemlich (*17*) introduced a nonfoaming bubble fractionation technique to separate dissolved surface-active materials such as dyes from solutions. They provided a useful conceptual framework for evaluating the separation process. However, quantitative testing of the method was not demonstrated because the eddy dispersivity was not measured. In our work, all parameters were independently determined. We also improved the column design of Lemlich (*15*) by increasing the air–water interfacial area per unit volume of solution. This improved the sensitivity of the method and made it possible to generate measurable concentration gradients of less surface-active species such as clays, bacteria, and humic acids.

In a bubble fractionation column at steady-state, the local mass balance for a surface-active compound requires that the upward and downward transport rates be equal (*15*). This condition is represented by

$$af\Gamma = AD\frac{dC}{dz} \quad (1)$$

where a is the surface area per bubble, f is the bubble generation rate, Γ is the surface excess, A is the column cross-sectional area, D is the column eddy dispersion coefficient, C is the concentration in solution (suspension), and z is the

* Corresponding author fax: (510)486-7797; e-mail: jwan@lbl.gov.

S0013-936X(98)00228-4 CCC: $15.00
Published on Web 09/04/1998

vertical coordinate (symbol definitions and dimensions are provided at the end of this paper). For dilute solutions (suspensions) in which partitioning at the water–gas interface is linear with respect to concentration, the surface excess is given by

$$\Gamma = KC \tag{2}$$

For surface-active molecules, K is the linear adsorption isotherm coefficient. The magnitude of K represents the thickness of the bulk solution that contains the same mass of surface active substance as is associated with the interface. To test the bubble column model, experiments within the linear range of K for the surfactant SDBS were performed, as described later. In extending this approach to particulate systems, we define K as the particle partition coefficient, relating particle surface excesses to their bulk suspension concentrations. The extension of eq 2 to linear partitioning of particles is intended to apply in dilute suspensions, when K is relatively constant. It is expected that in many natural systems the suspended colloid concentration will be sufficiently dilute such that the linear K approximation can be useful. The extension of this model to nonlinear colloid partitioning is outside the scope of this study. The solution to eqs 1 and 2 is an exponential profile, and the steady-state ratio of the concentration at elevation z versus at the bottom of the column is

$$\frac{C(z)}{C_b} = \exp(Jz) \tag{3}$$

where

$$J = \frac{afK}{AD} \tag{4}$$

and C_b is the concentration at the bottom of the column at steady-state. The constraint of mass conservation within the column provides the relation between C_b and the initial (also average) concentration C_o. Integration of eq 3 over the column height H and equating this result with HC_o gives

$$C_b = \left[\frac{HJ}{\exp(HJ) - 1}\right] C_o \tag{5}$$

such that

$$\frac{C(z)}{C_o} = \left[\frac{HJ}{\exp(HJ) - 1}\right] \exp(Jz) \tag{6}$$

Thus, measurement of the steady-state column profile of a solute or colloid permits determination of the separation parameter J. When A, a, f, and D have been independently determined, measurement of steady-state $C(z)$ permits determination of K. The accuracy with which K can be determined with the bubble column method is largely limited by uncertainties in the rate of interfacial area generation (the product af), as will be discussed later.

It should be noted that the above analysis applies throughout the bulk region of the bubble column but generally not at the very top surface. The boundary conditions at the upper surface of the column are complicated by the three-phase meniscus contact (bubble solution, air, and column wall) and liquid film adsorbed on the column wall immediately above the meniscus. This narrow surface zone is beyond the region of aggressive mixing by rising bubbles and, therefore, permits accumulations of surface active species at levels higher than predicted by eq 6.

Determining the Column Eddy Dispersivity. Among the aforementioned parameters requiring independent determination, only the eddy dispersivity (D) is experimentally difficult to quantify. To our knowledge, direct measurements of dispersion coefficients within bubble columns have not previously been reported. In this study, D was directly determined through measuring dispersion of step inputs of salt tracers in bubble columns. The analytical solution from the analogous heat flow problem was presented in Carslaw and Jaeger (*18*). When a salt solution slug with size equivalent to an incremental column length L_Δ, at a concentration C_* is added instantaneously to one end of a bubble column (initially free of the tracer), the time-dependent concentration profile is given by

$$\frac{C(y,t)}{C_*} = (1 - y_1) - \frac{2}{\pi}\sum_{m=1}^{\infty}\left\{\frac{1}{m}\cos(m\pi y)\,\sin(m\pi y_1)\,\exp\left[\frac{-m^2\pi^2 Dt}{H^2}\right]\right\} \tag{7}$$

where $y = z/H$, $y_1 = z_1/H$, and z_1 is the length of the initially solute-free section of the bubble column ($H = z_1 + L_\Delta$). The experimental determination of bubble column dispersion coefficients described later involves optimizing D in eq 7 to obtain best fits to salt concentration profiles.

Verification of the Bubble Column Method. To verify the uniqueness of the bubble column results, adsorption isotherm constants obtained with the bubble column method can be compared with values obtained by surface tension (γ) measurements. For a dilute surfactant solution, combining the Gibbs adsorption equation

$$\Gamma = -\frac{C}{RT}\frac{d\gamma}{dC} \tag{8}$$

with eq 2 gives

$$K = \frac{-1}{RT}\frac{d\gamma}{dC} \tag{9}$$

where R is the gas constant and T is the Kelvin temperature. Thus, whether surface excesses measured by bubble column and surface tension measurements are equivalent can be tested in simple surfactant solutions through comparing K values obtained using eqs 4 and 6 versus using eq 9.

Materials and Methods

Bubble Column. The column dimensions (2.0 m tall, 0.019 m i.d.) were chosen based on a compromise between maximizing top to bottom concentration differences (the longer the column the larger the difference) and easy laboratory operation (Figure 1). The bottom of the glass column is a 5 mm high air chamber, with a ceiling made of a fine-grade fritted glass plate (GM Associates, Inc., Oakland, CA). To maximize bubble concentrations, the area of the fritted glass plate was made larger than the area of the column cross section. Eight septum-capped sampling ports were distributed along the length of the column with shorter intervals toward the top end. The column was filled with a dilute solution (suspension) of surfactant (particles). Filtered compressed air was injected from the air chamber below the fritted glass plate, resulting in bubbles rising through the water column. Air flow was controlled and measured with a flow control system (E-32915-80, Cole-Parmer). A pressure transducer was used for monitoring the back pressure in the air chamber. An air flow rate range from 5 to 10 standard mL min^{-1} gave relatively high bubble populations without creating very large bubbles and rapid bubble streams for the given column conditions. Bubble diameters were measured photographically for each solution (suspension) type. A 20 mm by 15 mm flat glass window section was installed at the midcolumn section for photographing. For scale, a 254 μm diameter wire was installed in the windowed portion of the column, away from the glass wall. Photographs were taken

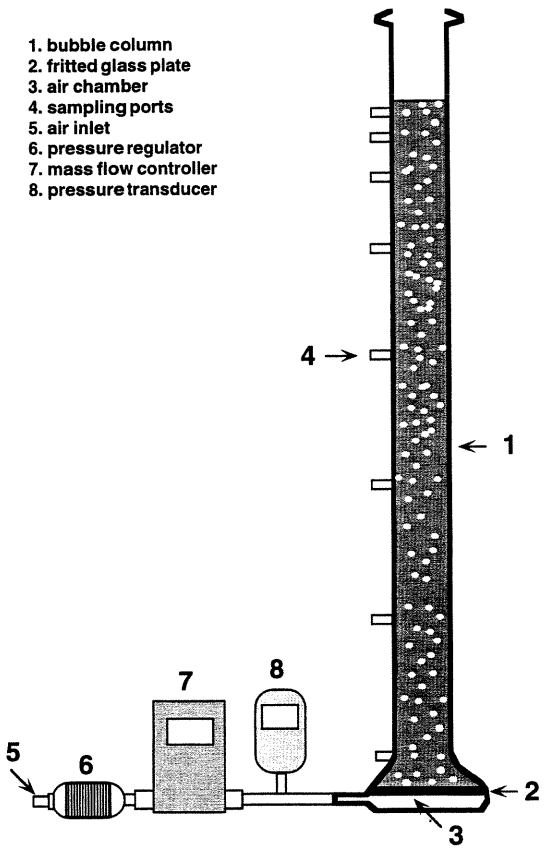

FIGURE 1. Bubble column device.

under the standard air flow rate, with a fast shutter speed (1/1000 s). For a given solution (suspension), the total surface area of >250 photographed bubbles was calculated (assuming spherical symmetry), from which an area-averaged bubble diameter was determined. The time required to reach the steady state was experimentally predetermined by sampling every 30 min. After the measurements were obtained, the withdrawn samples were carefully re-injected back into the column through their respective sampling ports in order to keep the water level within the column practically unchanged. The small disturbances due to sampling and re-injection diminished quickly. Results showed that a range from 1 to 3 h was needed to reach steady state. A notable mass loss was observed when a column experiment was conducted for too long (>8 h). We ran all the column experiments in this study for 3 h.

A surfactant, salt, and two types of colloids were tested for surface activity with the bubble column. These were sodium dodecyl benzene sulfate (SDBS, Aldrich), NaCl, kaolinite clay (KGA1b, well-crystallized, Source Clay, Columbia, MO), and soil humic acid (HA, 1S102H, International Humic Substances Society, St. Paul, MN), respectively. The surfactant SDBS was selected to test the bubble column method, with concentrations ranging from 1.0×10^{-6} to 5.0×10^{-5} M, dissolved in 1.0 mM NaCl at pH 5.7. SDBS was chosen as the test surfactant since it is less foaming than many other surfactants at these concentrations. Since simple salts are excluded from the air–water interface, separate experiments with NaCl solutions (0.53 M) were conducted in order to test whether solute exclusion can be measured in the bubble column. Suspensions of kaolinite were prepared by size fraction using centrifugation. A narrow range of sizes (0.6–1.0 μm) was used for compatibility with the particle counting method used in this work. Kaolinite was tested at concentrations of 10^6, 10^7, and 10^8 particles mL^{-1}, in a solution of 1.0 mM NaCl and 0.5 mM $CaCl_2$ at pH 5.6–5.8. Kaolinite clay was used as supplied without any additional treatment. The three humic acid (HA) solutions used in the bubble column contained 4, 10, and 20 mg L^{-1} HA, respectively, in 5.0 mM Na_2SO_4 at pH 6.0. All experiments were conducted at 22.8 ± 0.5 °C, for 3 h to ensure that steady state was reached. Longer run times were not necessarily better since particle aggregation can also occur. At steady state, samples (1.5 mL each) were withdrawn through the sampling ports using syringes, in the order of top to bottom. A sample of the poorly mixed top surface of the column was also taken using syringe needle along the three-phase meniscus contact line. Concentrations of all samples including SDBS, kaolinite, and humic acid were measured with a spectrophotometer (Milton Roy 601, Rochester, NY). The absolute particle numbers of clay colloids were determined using a particle analyzer (Coulter Multisizer II, Coulter Co., Miami, FL). The measured concentration profiles were used with the model (eq 6) to obtain surfactant adsorption isotherm constants and colloid partition coefficients, K.

To test the bubble column method, the K value of SDBS was determined using an independent approach, through surface tension measurements. The surface tension measurements were conducted with a Wilhelmy plate tensiometer (Kruss) at 22.8 ± 0.5 °C. Solutions containing up to 1.0×10^{-4} M SDBS (in 1.0 mM NaCl, at pH 5.7) were measured. We also tried to measure the surface tension changes of HA solutions and found that they were not reproducibly measurable at concentrations of 10–20 mg L^{-1} and not detectable at 4 mg L^{-1}. Kaolinite suspensions exhibited no measurable surface tension changes.

Eddy Dispersivity. To directly determine the eddy dispersion coefficient, measurements of transient salt mixing were made in the bubble column. For these measurements, six conductance electrodes were installed in the column through the sampling ports (excluding the sampling port near the tracer injection point) and connected to a data logger (CR7, Campbell Scientific Inc., Logan, UT). A potassium chloride solution (0.1 M, 3 mL) containing blue dye was injected into the bottom of the column containing deionized water. The color dye was included in the KCl solution in order to determine the boundary of the tracer immediately after injection. Air flow (at a constant rate) was initiated immediately after the location of the tracer solution boundary was determined. Time zero was recorded as the air bubbles emerged within the source area of the tracer solution. Conductivity data from all six electrodes were recorded simultaneously at 20-s intervals until steady state was reached. The analytic solution of dispersion equation (eq 7) was then fit to each of the six measured time-dependent conductivity profiles by adjusting the dispersivity, D, the only fitting parameter. An average of six best fit D values was used as the representative column eddy dispersivity under the given combination of column dimensions, flow rate, and bubble size. It is worth noting that, besides testing by injecting the tracer solution from the bottom of the column, we also tested by adding the tracer solution at the top of the column. The measured average D from the top source and the bottom source were essentially the same, but the top-source method had larger uncertainties because a clear and stable boundary between the tracer solution and the deionized water was difficult to establish at time zero. Therefore bottom injection is recommended for determinations of D.

Results and Discussion

Dispersivity. Examples of normalized conductivity data obtained for determinations of D are shown in Figure 2. The results shown are from a run using an air flow rate of 10.0 mL min^{-1}. Points are normalized conductance data, and lines are model results based on eq 7. Electrode R1 was located farthest away from the tracer source, and electrode

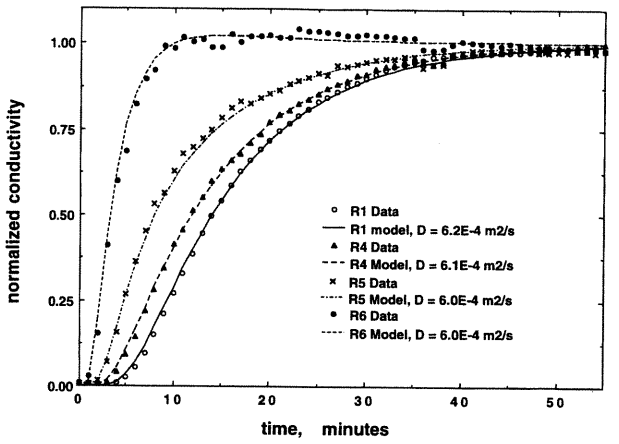

FIGURE 2. Eddy dispersivity measurements. Measured time-dependent conductivity data at air flow rate of 10.0 mL min^{-1} from electrodes assembled along the column. Electrode R1 is located furthest away from the tracer source, and electrode R6 is closest to the tracer source.

TABLE 1. Bubble Size Measurements

	NaCl (M)	pH	no. measured	av diam (μm)
SDBS 1.5 × 10^{-5} M	1.0 × 10^{-3}	5.7	469	347
kaonilite 1 × 10^{-7} mL^{-1}	1.0 × 10^{-3}	5.7	302	641
	1.0 × 10^{-3}	3.9	326	638
	1.0 × 10^{-1}	5.7	663	539
colloid-free	1.0 × 10^{-3}	5.7	267	645
	1.0	5.7	700	439

[a] At air flow rate 10.0 mL/min.

R6 was the one closest to the tracer source. Data from electrodes R2 and R3, located between R1 and R4, are not shown. The calculated D from each plotted elevation are presented in the figure legend. Not shown in the figure legend are the best-fit D of 6.2 × 10^{-4} m^2 s^{-1} obtained for both R2 and R3. The measured D at air flow rates of 7.0 and 10.0 standard mL min^{-1} were essentially identical and only slightly lower at the 5.0 mL min^{-1} flow rate, indicating that the column D was not very sensitive to flow rate changes in the range tested. Therefore, an air flow rate of 10.0 mL min^{-1} and a D value of 6.1 × 10^{-4} m^2 s^{-1} were used in the rest of this study. On the basis of all measurements, a relative uncertainty of 0.1 was associated with D in later calculations of K.

Bubble Size. The measured average bubble diameters under different solution (suspension) conditions and a fixed air flow rate are listed in Table 1. It was found that bubbles were significantly smaller in surfactant solutions than in surfactant-free colloid suspensions. No significant differences in effective bubble size were measured between dilute clay suspensions and particle-free solutions with the same salt concentration. Ionic strength had a large effect on bubble size. Bubbles were significantly smaller in the 1.0 M NaCl solution than in the 1.0 mM NaCl solution. It was also observed that more large bubbles appeared in the upper region, and finer bubbles were more abundant at the bottom region. A 10% increase in bubble size is expected in rising from the bottom to the top of the column due to the decrease in pressure along the column length. Some additional increases in bubble size toward the top region of the column occurred due to merging of bubbles.

Uncertainty in Partition Coefficients. Uncertainties in calculated values of K depend directly on uncertainties in J, A, D, a, and f (eq 4). The relative uncertainty in D was discussed in the previous section. The uncertainty in J reflects

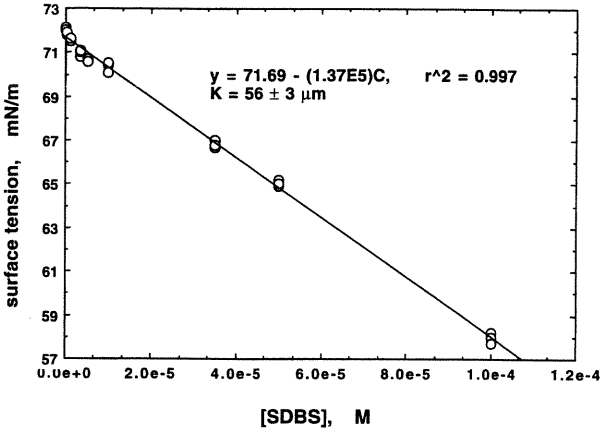

FIGURE 3. Surface tension of aqueous solutions versus SDBS concentrations.

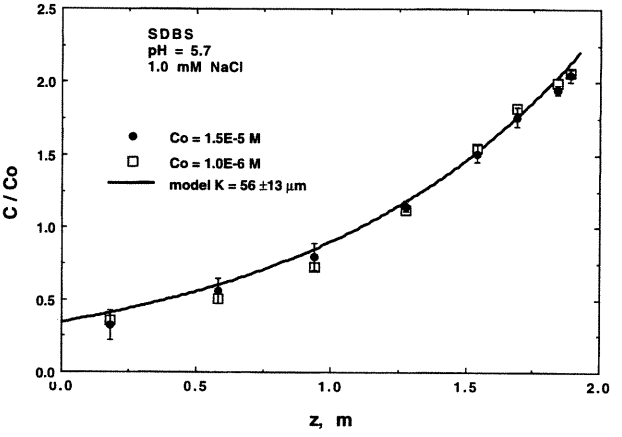

FIGURE 4. Steady-state relative concentration profiles of SDBS in the bubble column. Data points are from column experiments conducted at the two indicated average SDBS molar concentrations.

the reproducibility with which the steady-state $C(z)/C_b$ profile can be fit to the exponential function (eq 3). This reproducibility in J was within ±10%, based on replicate runs. The relative uncertainty in A was negligible relative to all other factors. As noted previously, the product af, which represents the interfacial area generation rate, is the largest source of uncertainty. The uncertainty in af is due to uncertainties in bubble size distribution and to bubble surface area increases during their traverse through the column. The relative uncertainty in af due to all of these factors was estimated at 0.2, resulting in a composite relative uncertainty for K of 0.24.

Testing the Bubble Column Method

The dependence of surface tension on SDBS concentrations is shown in Figure 3. These results show a constant slope of −1.37 ±0.07 × 10^5 (mN/m)/M, for SDBS concentrations up to 1.0 × 10^{-4} M, with the uncertainty based on triplicate measurements. This range of SDBS concentrations encompasses that used in the bubble column experiments. Combining the aforementioned slope of the SDBS surface tension-concentration function with eq 9 yielded a K of 56 ± 3 μm. This value of K was then compared with results obtained for SDBS in the bubble column. Steady-state profiles of SDBS concentrations in the bubble column are shown in Figure 4 (data for 1.0 × 10^{-6} M SDBS represent averages of triplicate runs), along with best fit K of 56 ± 13 μm. The ±13 μm in the bubble column K is largely due to the uncertainty in the interfacial area generation rate, af, as previously described. This K value for SDBS from the bubble column is in fair

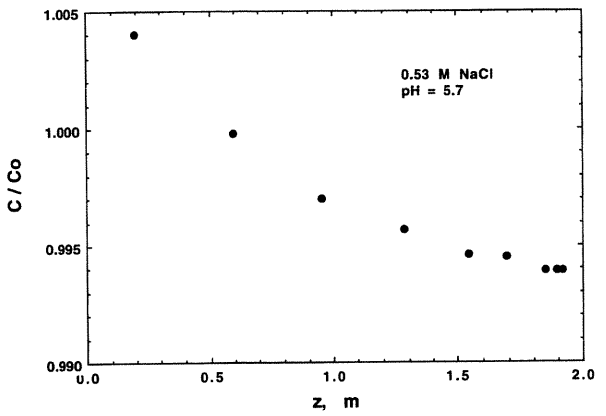

FIGURE 5. Steady-state relative concentration profile for NaCl in the bubble column. The average column NaCl concentration is 0.53 M.

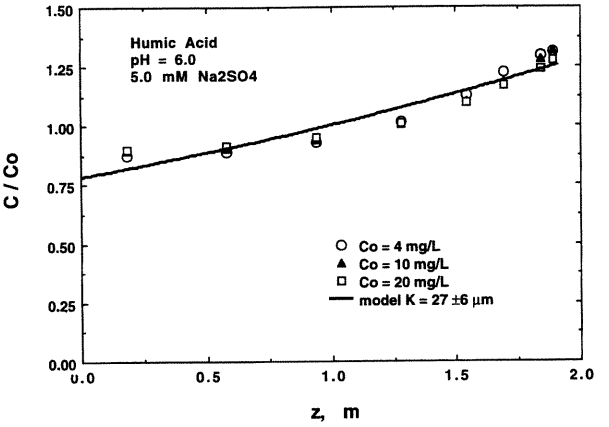

FIGURE 6. Steady-state relative concentration profiles of humic acid in the bubble column. Data points are from column experiments conducted at the three indicated average HA concentrations.

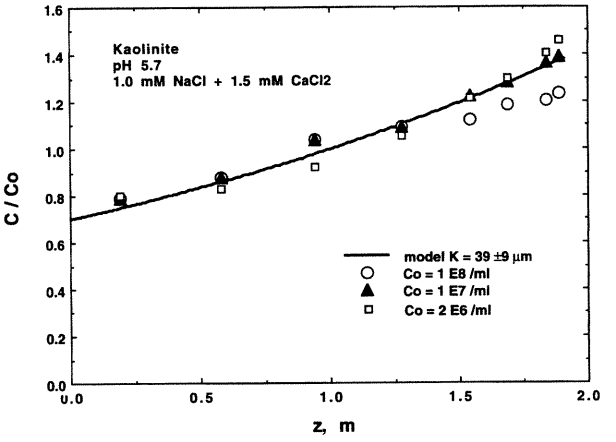

FIGURE 7. Steady-state relative concentration profiles of kaolinite clay particles in the bubble column. Data points are from column experiments conducted at the three indicated average clay concentrations.

agreement with the K (56 ± 3 μm) obtained from surface tension measurements. This agreement validated the bubble column technique as a method for determining partitioning of surface-active components at air–water interfaces.

It is worth mentioning that a small body of foam accumulated at the top of the column. At the higher concentration of SDBS ($C_o = 1.5 \times 10^{-5}$ M), a steady-state foam layer up to 20 mm in thickness built up at the top of the water column. It is also a general feature for all the measured surface-active colloids that a discontinuity in concentrations develops at the top of the column, with much greater enrichment at the surface layer. The surface does not mix efficiently with the bulk column, resulting in more accumulation of surface-active species relative to the immediately underlying bulk suspension. Furthermore, reproducible sampling of this surface layer using a syringe needle is not possible. However, because the ratio of the top surface area relative to the column length is small, the total mass loss is minor. Since the top surface region did not mix effectively with the bulk column, data from the surface were excluded from the model fits. For purposes of calculating K values, steady-state concentrations along the column length were normalized to recovered column average concentrations.

Like other simple salt solutions, the surface tension of NaCl solutions increases with concentration (*11*). Thus, negative concentration gradients of simple salts are expected to develop in bubble columns. For a 0.53 M NaCl solution [surface tension 73.57 mN/m at 25 °C (*19*)], the measured steady-state concentration at the top of our bubble column was 1.0% less than that at the bottom (Figure 5). Although salt exclusion can be identified in the bubble column, a model for quantifying exclusion remains to be developed.

Surface Partition Coefficient Measurements of Colloids. Steady-state bubble column profiles (measured and modeled) for humic acid and kaolinite are shown in Figures 6 and 7, respectively. Both of these systems clearly exhibited concentration gradients, with preferential partitioning of humic acid and kaolinite at the air–water interface. The mechanisms responsible for colloid partitioning at the air–water interface are beyond the scope of this paper. It is expected that colloid surface chemistry and solution chemistry will have strong influences on partitioning at gas–water interfaces.

The measured relative concentration profiles of HA from the bubble column and the best-fit model profile are shown in Figure 6. The results indicate that the bubble column method gives reproducible measurements of HA partitioning at air–water interfaces. However, the model profile using a single value, best-fit K of 27 ± 6 μm overpredicts separation in the lower region and underpredicts separation in the upper region of the column. This may be due to the HA samples being composed of a mixture of macromolecules that exhibit a range of surface activity. We are not aware of any reports of surface tension-based measurements of HA surface excesses at such low concentrations. Given the extremely wide range of reported values of molecular weights for HA (*19*), it was not possible to report either bulk or surface concentrations on a number or molar basis. Nevertheless, our measured K permit determination of HA surface excesses in terms of mass per interfacial area. The distinct concentration gradient and the reproducible values obtained in the bubble column demonstrate the potential usefulness of this method in studies of surface excesses of humic colloids and their complexes with other species.

Measured relative concentration profiles of kaolinite and the best-fit model profile are shown in Figure 7. The well-developed concentration gradients for kaolinite in the bubble column demonstrated that, under the given solution chemistry, this clay partitions favorably at air–water interfaces despite the lack of measurable changes in surface tension. Over a 2 order of magnitude range in concentrations, the clay suspensions gave a fairly linear partitioning relation, although the data show slightly higher separation efficiencies at lower concentrations. A K value of 39 ± 9 μm accounted for kaolinite partitioning over the tested range of suspension concentrations. When clay suspension concentrations are expressed in terms of mass per unit volume, surface excesses

of clays are identified in terms of mass per interfacial area. Since experiments with kaolinite included quantification of suspension concentrations in terms of particle numbers per unit volume, it was possible to express surface excesses in terms of the number of colloids per interfacial area. Surface excesses (eq 2) ranged from 80 to 4000 particles mm^{-2} (10^4–300 μm^2 per particle) for the three kaolinite suspension concentrations.

Vadose Zone Implications. With this new ability to measure colloid surface excesses, more quantitative analysis of a wide variety of environmental processes becomes possible. Implications of these types of measurements are especially relevant in the vadose zone because this portion of the environment can have high values of air–water interfacial area per unit bulk volume. Furthermore, due to the common existence of thin water films in the vadose zone, the distribution of surface-active colloids between bulk water and the air–water interface can become very significant. In partially water-saturated soil, the mass of colloidal material associated with air–water interfaces, N_Γ, relative to their mass in aqueous suspensions, N_s, can be estimated. From eq 2 it follows that

$$\frac{N_\Gamma}{N_s} = K\frac{A_s}{V_w} \tag{10}$$

where A_s/V_w is the air–water interfacial area per volume of soil water. The inverse of this ratio is the effective thickness of water films in partially saturated soils (averaged over both true water films and pendular water around grain–grain contacts), typically ranging from nanometers up to about 100 μm. Given the K values ranging from 27 to 39 μm for humic acid and kaolinite, respectively, eq 10 indicates that the amount of interface-associated colloids is of the same order as that in suspension in partially saturated soils (under similar solution chemistries). This result indicates that colloid partitioning at air–water interfaces of partially saturated porous media can be much more significant than previously recognized. It should be noted that eq 10 does not apply when film thicknesses are less than or equal to characteristic colloid sizes. Under these conditions, air–water interfaces are retracted onto hydrophilic colloids (*20*), and colloids are in contact with air–water interfaces regardless of their K values.

Acknowledgments

This work was carried out under U.S. Department of Energy Contract DE-AC03-76SF-00098. Funding was provided by the U.S. Department of Energy, the Environmental Management Science Program. We appreciate the technical support provided by Dr. Rohit Salve and Jenny Yang and helpful review comments by Drs. Fred Gadelle and Srinivas Veerapaneni of LBNL and by anonymous reviewers. We also thank the Swedish Nuclear Fuel and Waste Management Company, SKB, for providing some initial support for this study.

Notation

A	cross-sectional area of bubble column (L^2)
A_s	air–water interfacial area in soil (L^2)
a	surface area per bubble (L^2)
C	concentration in solution (suspension) ($M\ L^{-3}$)
C_0	initial (and average) concentration ($M\ L^{-3}$)
C_b	steady-state C at the column bottom ($M\ L^{-3}$)
D	column eddy dispersion coefficient ($L^2\ T^{-1}$)
f	bubble generation rate (T^{-1})
H	column height (L)
J	column separation parameter (L^{-1})
K	linear adsorption isotherm coefficient (L)
N_Γ	number of colloids at the air–water interface ( )
N_S	number of colloids in suspension ( )
R	gas constant ($M\ L^2\ T^{-2}\ mol^{-1}\ K^{-1}$)
T	Kelvin temperature (K)
t	time (T)
V_w	volume of soil water (L^3)
z	vertical coordinate (positive upward) (L)
Γ	surface excess ($M\ L^{-2}$)
γ	surface tension ($M\ T^{-2}$)

Literature Cited

(1) Sutcliffe, W. H.; Baylor, E. R., Jr.; Menzel, D. W. *Deep-Sea Res.* **1963**, *10*, 233–243.
(2) Duce, R. A.; Quinn, J. G.; Olney, C. E.; Piotrowicz, S. R.; Ray, B. J.; Wade, T. L. *Science* **1972**, *14*, 161–163.
(3) MacIntyre, F. *Sci. Am.* **1974**, *230*, 62–77.
(4) Gershey, R. M. *Limnol. Oceanogr.* **1983**, *28*, 309–319.
(5) Lewis, B. L.; Landing, W. M. *Mar. Chem.* **1992**, *40*, 105–141.
(6) Skop, R. A.; Viechnicki, J. T.; Brown, J. W. *J. Geophys. Res.* **1994**, *99*, 16395–16402.
(7) Chen, Y.; Schnitzer, M. *Soil Sci.* **1972**, *125*, 7–15.
(8) Wan, J.; Wilson, J. L. *Water Resour. Res.* **1994**, *30*, 11–23.
(9) Wan, J.; Wilson, J. L.; Kieft, T. L. *Appl. Environ. Microbiol.* **1994**, *60*, 509–516.
(10) Powelson, D. K.; Mills, A. L. *Appl. Environ. Microbiol.* **1996**, *62*, 2593–2597.
(11) Hiemenz, P. C. *Principles of Colloid and Surface Chemistry*, 2nd ed.; Marcel Dekker Inc.: New York, 1986.
(12) Blanchard, D. C.; Syzdek, L. *Science* **1970**, *170*, 626–628.
(13) Gershey, R. M. *Limnol. Oceanogr.* **1983**, *28*, 395–400.
(14) Blanchad, D. C. *Estuaries* **1989**, *12*, 127–137.
(15) Lemlich, R. *AIChE J.* **1966**, *12*, 802–804.
(16) Lemlich, R. In *Recent Developments in Separation Science*; Li, N. N., Ed.; The Chemical Rubber Co.: Cleveland OH, 1972.
(17) Shah, G. N.; Lemlich, R. *Ind. Eng. Chem. Fundam.* **1970**, *9*, 350–355.
(18) Carslaw, H. S.; Jaeger, J. C. *Conduction of Heat in Solids*, 2nd ed.; Oxford Clarendon Press: Oxford, 1959.
(19) Ronald, B.; Bigelow, J. C.; Zhang, J.; Giddings, J. C. In *Aquatic Humic Substances*; Suffet, I. H., MacCarthy, P., Eds.; American Chemical Society: Washington, DC, 1989.
(20) Wan, J.; Tokunaga, T. K. *Environ. Sci. Technol.* **1997**, *31*, 2413–2420.

Received for review March 10, 1998. Revised manuscript received July 20, 1998. Accepted July 28, 1998.

ES980228A